

High-Throughput Search and Prediction of Layered 4f-Materials

Lin Hou,¹ Ying Wai Li,² and Christopher Lane^{1,*}

¹*Theoretical Division, Los Alamos National Laboratory, Los Alamos, New Mexico 87545, USA*

²*Computer, Computational, and Statistical Sciences Division,
Los Alamos National Laboratory, Los Alamos, New Mexico 87545, USA*

(Dated: September 10, 2024)

The development of multifunctional devices calls for the discovery of new layered materials with novel electronic properties. f-electron systems naturally host a rich set of competing and intertwining phases owing to the presence of strong spin-orbit coupling, electron-electron interactions, and hybridization between itinerant and local electrons. However, very little attention has been devoted to exploring the f-electron family of compounds for new promising layered material candidates. Here, we identify 295 rare earth compounds from across the lanthanide series of elements that exhibit a spectrum of lattice symmetries and electronic properties. In particular, we find metallic compounds and insulating systems with band gaps covering a 0.1 eV to 5.3 eV range which opens new possibilities in infrared quantum sensors, designer photocatalysts, and tunable transistors. The inclusion of 4f-states in a layered system also suggests the possibility of 2D confined heavy-fermion superconductivity and topological semimetals. Our study serves as a springboard to further systematic theoretical investigation of correlation-driven properties of the 4f and other 2D materials composed of heavy elements.

INTRODUCTION

For the past 50 years modern microelectronics, signal processing devices, and data storage technologies have relied on simple metals and semiconductors to provide an exponential growth in processing power that has enabled exceptional leaps in fundamental science, engineering, and communications. However, in the last 15 years computational power has begun to saturate and, with it, Moore’s Law is leveling off[1]. The choke point limiting data bandwidth, and ultimately high-throughput information processing, is the limited electronic properties of the underlying conventional materials of the integrated circuits[2, 3]. To overcome these intrinsic limitations and enable new complex integrated devices, new materials hosting rich multifunctional properties are required.

Layered materials are solids with highly anisotropic bonding, i.e. strong covalent bonds within the layers and weak van der Waals type bonds connecting adjacent layers. These systems cover a wide range of novel electronic[4], excitonic[5], valley[6], topological physics[7] that may be tuned to a high degree via doping[8], electrostatic gating[9], and defect engineering[10, 11]. Theoretical materials discovery efforts have concentrated on discovering new layered materials composed of various s-, p-, d-block elements, yielding \sim 5,000 candidate compounds[12–16]. So far, several of these material families have been experimentally synthesized and characterized, including graphene, hexagonal boron nitride (hBN), black phosphorus, transition-metal dichalcogenides (TMDs), III-metal monochalcogenides and MXenes[17].

Compounds composed of heavy elements, such as those in the lanthanide and actinide series, expand the current landscape of layered materials by giving access to phe-

nomena at the intersection of strong spin-orbit coupling, electron-electron correlation effects, and the intertwining of local and itinerant states[18, 19]. Such systems offer intriguing possibilities for layer-confined unconventional superconductivity, non-trivial topology, and Kondo effects while simultaneously able to be miniaturized and embedded into industrially important semiconductors. A recent set of papers pursues the materialization of layered rare earth compounds by intercalating Eu into a graphite matrix[20] and rare earth doped 2D transition metal dichalcogenides[21], with a handful of cases examining crystalline compounds such as CeI₂[22], Ce₂Te₅[23], CeSiI[24–26], (Y,La,Ce)Te₃[27], Gd(I,Br,Cl,F)₂[28] and YbOCl[29]. However, progress in this area has been slow due to a lack of theoretical predictions of new 2D rare earth candidate materials[30].

In this article, we perform a search for all layered rare earth compounds from the major crystallographic databases and elucidate their structural and electronic properties. We identify 295 compounds that span 35 space groups, with each comprised five unique structure types on average. These materials are mainly composed of reactive nonmetals, metalloids, and a variety of lanthanide elements. Accordingly, a rich array of electronic behaviors are found, covering metallic, insulating, and four possible Z_2 topological insulators.

RESULTS AND DISCUSSION

We identify 295 layered 4f compounds sourced from the three major international materials databases: ICSD, COD, and MPDS, all of which are populated by experimental crystal structure data. A complete list of the layered compounds is given in the Supplementary Materials. Figure 1 presents the distribution of the element com-

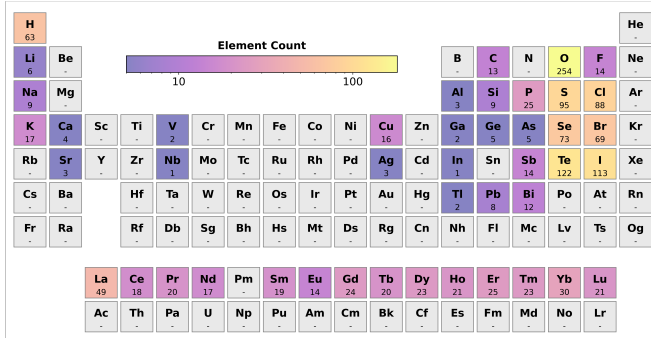


FIG. 1. (color online) Element distribution of all 295 identified layered 4f compounds plotted within the periodic table. The lighter color indicates a particular element is more prevalent, where each unique elemental species is counted once.

position of all identified compounds, where for a given material each unique elemental species was counted once. The 295 compounds are evenly distributed across the lanthanide series of elements, with the exception of Promethium (Pm), which poses challenges due to its radioactive nature. Notably, almost all systems feature oxygen, with significant contributions from hydrogen, and the non-metal and halogen elements. In contrast, only a few transition metals appear in very low frequency.

Commonly, correlated f-electron materials are intermetallic compounds that are composed of elements with 4f or 5f electrons and metals (including post-transition metals and metalloids). These materials typically host three-dimensional (3D) bonding networks and consequently are not layered and hard to cleave. However, if high electronegativity atomic species are introduced, such as hydrogen, chalcogens, halogens, and other non-metal elements, they are able to occupy interstitial sites and encapsulate the 4f or 5f electrons and metallic elements, hence promoting a layered crystal structure. This process explains the significant presence of oxygen and hydrogen in Fig. 1.

Though transition metals play a minor role in the identified layered 4f compounds, their inclusion introduces additional electronic degrees of freedom. This expanded space of competing and intertwining interactions further enrich the electronic and magnetic properties of the system. Moreover, they offer opportunities for doping and functionalization, enabling further tailoring of the material's properties for specific applications. However, just a few compounds containing transition-metal ions appear in our search, suggesting the potential for the synthesis and prediction of new materials.

Structure Analysis

Figure 2(a) presents a frequency distribution of the 295 layered 4f compound space groups. The distribution is

highly concentrated in a few space groups, with most representing less than five crystals. Specifically, space group #129 exhibits the highest frequency of occurrence among the compounds, with space groups #63, and #166 following closely in number. These crystal systems cover the tetragonal, orthorhombic, and trigonal families, respectively, and are consistent with layered systems that typically exhibit large c/a ratios and staggered stacking configurations. All together, these three space groups alone account for nearly 40% of the total number of compounds.

The layered compounds in each space group are further categorized according to their structural similarities, where all species are considered indistinguishable and we focused only on the presence and multiplicity of Wyckoff positions in the unit cell. The inset in Fig. 2(a) shows the break down of structure types for each space group with their multiplicity. We find the majority of space groups to host about five distinct structure types, indicative of structural diversity within each crystal class. Curiously, the compounds with space group #148 are all of the same structure type. Additionally, we sought to identify special lattice structures such as the kagome, Lieb, and pyrochlore lattices among the 295 compounds; however, our analysis did not yield any instances of these specific lattice types within our dataset.

Figure 2 (b) shows the distribution of point groups in all 295 layered 4f compounds for rare earth, transition metal, and remaining elements. To facilitate comparison, each distribution is normalized to unity. Most point groups are represented in each set, with notable exception: all cubic point groups are absent from the set of layered compounds. The transition metals are mainly clustered around $.m.$, $4mmm$, and $mm2$ point groups, with the rare earth elements approximately evenly spread across various site symmetries. The distribution of the remaining elements are concentrated at the 1 and $.m.$ site symmetries. Interestingly, the leading point groups found in the broad set of two-dimensional layered materials[12], such as $-3m$, $2/m$, and -1 , are marginal for the layered 4f compounds. Furthermore, while most of the layered materials studied in the last ten years belong to the hexagonal crystal system, these structures represent only a minority of the full set of layered 4f compound.

A key problem that arises in integrating new materials into existing devices is lattice and chemical matching. Importantly, a wide range of layered and 2D materials, including graphene, transition metal dichalcogenides, hexagonal boron nitride, have demonstrated success in integrating with silicon and other industrially important semiconductors[31–33]. This suggests, our broad set of layered materials may expand the set of integrable layered materials to enrich the properties of current device technologies.

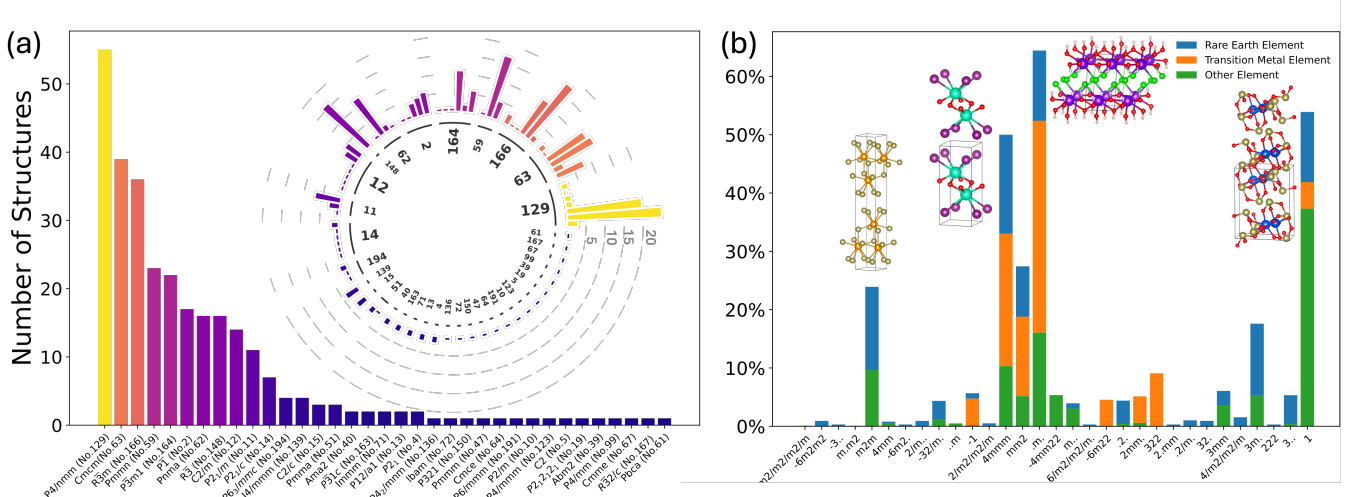


FIG. 2. (color online) (a) Space group frequency distribution for all 295 layered 4f-material crystal structures. The inset is a break down of unique structure types for each space group with their corresponding multiplicity. (b) Distribution of point groups in all 295 layered 4f compounds for rare earth, transition metal, and remaining elements. Each distribution is normalized to unity.

Electronic Properties

Unlike s-, p-, and d-electrons that can readily diffuse throughout the material, f-electrons tend to be localized around their atomic center with minimal hybridization with the rest of the system. As a consequence, the f-electron states experience strong correlation effects that can drive a variety of novel phenomena including superconductivity, magnetism, and the Kondo effect. This behavior makes such systems hard to model within standard electronic structure approaches and typically requires higher-level theory to accurately capture their behavior. To provide a baseline of insight into the electronic properties of the 295 layered 4f materials, we performed high-throughput all-electron DFT calculations with the f-levels treated as core and valence electrons, to account for both localized and itinerant f-electron scenarios, respectively. Additionally, to mark the effect of relativistic corrections, calculations were performed with and without spin-orbit coupling.

Figure 3 presents the distribution of electronic band gaps of the 295 layered 4f materials where direct, indirect, and zero (metal) band gaps are indicated in red, blue, and yellow color semicircles. Specifically, in Fig. 3 (a) and (b), we compared the impact of including spin-orbit coupling for f-electrons located in the core and valence, respectively, and in Fig. 3 (c) and (d) compare the effect of open and closed core configurations in the presence of spin-orbit coupling and no relativistic effects, respectively.

In Fig. 3 (a), the inclusion of spin-orbit coupling reduces the band gap by approximately 0.1 eV on average with minimal changes in the band gap type. Interest-

ingly, direct band gap compounds are concentrated near 0.2 eV and 4.8 eV, while those with indirect band gaps are evenly spread between 0.1 eV and 5.2 eV. Despite the removal of the f-electrons from the Fermi level, most materials exhibit metallic behavior regardless of the presence of spin-orbit coupling. Notably, a few systems gain a finite band gap upon the inclusion of spin-orbit coupling, thereby suggesting these materials to be non-trivial \mathbb{Z}_2 topological insulators.

When the f-electrons are included in the valence [Fig. 3 (b)], the effect of spin-orbit coupling is more pronounced for systems with small band gaps (< 1.5 eV), where some gaps are reduced by up to 50%. This sensitivity at small band gaps stems from the significant number of narrow f-electron bands at the Fermi level. Moreover, the presence of f-electrons in the valence leads to a substantial increase in metallic behavior. The distribution of direct and indirect bands gaps is similar to those in the open core calculations.

Figure 3 (c) and (d) display very similar features, suggesting that spin-orbit coupling plays a lesser role compare to the treatment of the f-electrons. Many materials transition to being metals, or exhibit an extremely reduced band gap, upon the inclusion of f-states in the valence. Notably, materials containing close/empty shell elements, such as La, experience no change in band gap, with minimal changes in band gap type. Interestingly, several compounds exhibit an increase in the band gap when the f-electrons are taken out of the core. These systems also display a significant sensitivity to including spin-orbit coupling effects.

A wide range of key applications spanning catalysis,

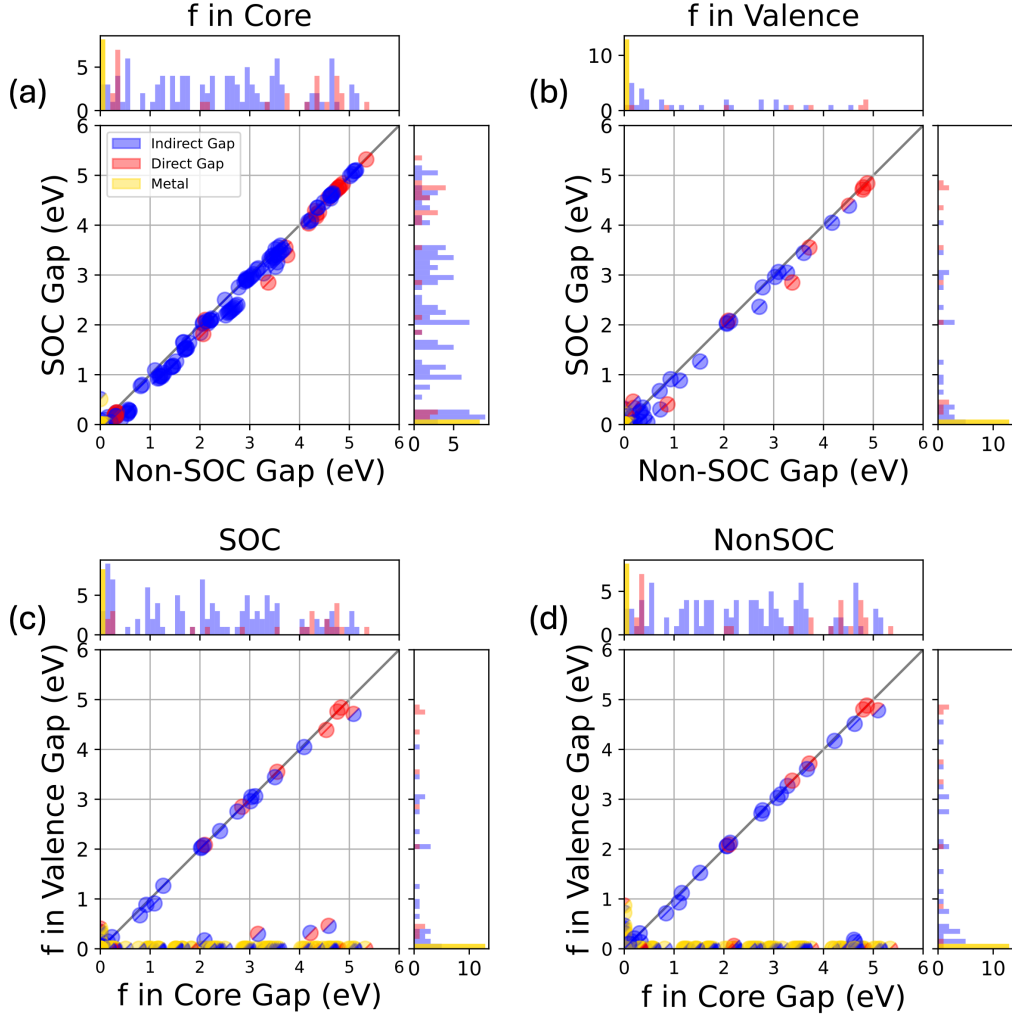


FIG. 3. (color online) (a) and (b) Comparison of electronic band gaps with and without spin-orbit coupling for f-electrons either located in the core or valence, respectively. (c) and (d) Comparison of electronic band gaps for f-electrons in the core and in the valence for spin-orbit coupling either turned on or off, respectively. Direct, indirect, and zero (metal) band gaps are indicated in red, blue, and gold color, respectively. The zero band gap contribution to the histograms is scaled by a factor of 0.1.

quantum sensors and emitters, and next-generation transistors, rely on the presence of energy band gap in the electronic states. 2D layered materials such as the transition metal dichalcogenides and hexagonal boron nitride have been the workhorse compounds over the past 10–15 years despite their intrinsic electronic band gaps only covering excitation in a 1–2 eV and ~ 6 eV window, with almost none otherwise. Here, we find by expanding the family of layered materials to include rare earth elements a range of band gap energies that cover 0.1 eV to 5.3 eV. This enlarged range of accessible band gaps opens up new opportunities in narrow band gap (infrared) quantum sensors, designer photocatalysts, tunable transistors and gates.

The identification of a large number of metallic sys-

tems raises the exciting possibility of new broken symmetry phases driven by the coexistence of correlations and strong spin-orbit coupling. In particular, the inclusion of 4f-states in a layered system suggests the possibility of 2D confined heavy-fermion superconductivity, topological semimetals, and strong crystalline anisotropy. Such attractive phases of matter when integrated on a chip opens up new avenues for enhanced mean-free paths, ultra-high conductivity, anisotropic conduction channels.

In summary, we have expanded the known family of layered materials by identifying 295 layered 4f-materials from the three major databases of experimental inorganic crystal structures. Importantly, these materials sit at the virtually unexplored intersection of strong spin-orbit coupling, electron-electron correlation effects, and

the hybridization of local electrons with conduction electrons. Furthermore, their properties expand the phase space of materials for quantum sensors and anisotropic conduction channels, necessary for advanced integrated circuits. Our study serves to stimulate new experimental synthesis and characterization, and theoretical analysis.

COMPUTATIONAL DETAILS

Density functional theory (DFT) calculations were performed using the full potential linearized augmented plane-wave+local orbitals (L/APW+lo) method[34, 35] as implemented in the WIEN2k code[36]. Exchange-correlation effects were treated by using the Perdew-Burke-Ernzerhof generalized gradient approximation (PBE-GGA) [37]. 1000 (2000) k-points were used to sample the Brillouin zone on a Γ -centered grid for unit cell with more than 3 (less than 4) atoms. An energy cutoff of -6.0 Ry was used to delineate the core-valence separation. The value of $R_{mt}K_{max}$ was chosen to vary with the size of the smallest atomic species in the unit cell, see Table 1 in the Supplementary Materials for details. Furthermore, we set lvns=10 and gmax=25 for materials with H. To gain insight into the sensitivity of the electronic structure to the treatment of relativistic effects and f-electron localization, we consider both non-spin-orbit coupling and finite spin-orbit coupling cases, and f-electrons in the valence and in the core via the open core method.[36]

To identify layered 4f-materials we must determine the various bonding subunits of a given crystal and their associated dimensionality. This is accomplished by constructing a bond graph and performing a spectral decomposition of the graph Laplacian. Specifically, from the bulk primitive cell of the 3D candidate a $3 \times 3 \times 3$ super cell is created. All interatomic distances are then evaluated and chemical bonds are heuristically identified as those for which $d_{ij} < r_i^{vdW} + r_j^{vdW} - \Delta$, where d_{ij} is the distance between two atoms i and j , r_i^{vdW} is the van der Waals radius of atom i as determined in Ref. 38 and Δ is a tolerance factor to account for the experimental variance in r_i^{vdW} . On average, Δ is 1.3 Å[12]. Once all bonds are identified, the adjacency matrix \mathbf{A} is constructed such that A_{ij} equals 1 if there is a bond between atoms i and j , otherwise 0. The Laplacian is then $\mathbf{L} = \mathbf{D} - \mathbf{A}$, where $D_{ii} = \sum_j A_{ij}$. The number of bonding units in the compound is the dimension of the Null space of \mathbf{L} , i.e. the number of zero eigenvalues, with the corresponding eigenvectors specifying the connected units. Finally, the dimensionality of each chemically bonded unit is equal to the rank of the matrix formed by all the vectors connecting a given atomic site to all other equivalent sites in the chemically connected unit in the supercell.

The above procedure was applied to all rare earth compounds from the three major international materi-

als databases: the Inorganic Crystal Structure Database (ICSD), the Crystallography Open Database (COD), and Materials Platform for Data Science (MPDS). To ensure integrity of our search, each material was pre-screened to ensure the structure is crystalline and is not a duplicate crystal structure, similar to Ref. 12 and 39.

DATA AVAILABILITY

The data that supports the findings of this study are available from the corresponding author upon reasonable request.

* laneca@lanl.gov

- [1] J. Shalf, Philosophical Transactions of the Royal Society A **378**, 20190061 (2020).
- [2] R. H. Havemann and J. A. Hutchby, Proceedings of the IEEE **89**, 586 (2001).
- [3] C. Murray, S. Guha, D. Reed, G. Herrera, K. Kleese van Dam, S. Salahuddin, J. Ang, T. Conte, D. Jena, R. Kaplar, *et al.*, *Basic Research Needs for Microelectronics: Report of the Office of Science Workshop on Basic Research Needs for Microelectronics, October 23–25, 2018*, Tech. Rep. (USDOE Office of Science (SC)(United States), 2018).
- [4] J. Kim, S. S. Baik, S. H. Ryu, Y. Sohn, S. Park, B.-G. Park, J. Denlinger, Y. Yi, H. J. Choi, and K. S. Kim, Science **349**, 723 (2015).
- [5] C. Pöllmann, P. Steinleitner, U. Leierseder, P. Nagler, G. Plechinger, M. Porer, R. Bratschitsch, C. Schüller, T. Korn, and R. Huber, Nature materials **14**, 889 (2015).
- [6] P. Rivera, K. L. Seyler, H. Yu, J. R. Schaibley, J. Yan, D. G. Mandrus, W. Yao, and X. Xu, Science **351**, 688 (2016).
- [7] A. Bansil, H. Lin, and T. Das, Reviews of Modern Physics **88**, 021004 (2016).
- [8] C. Lane, D. Cao, H. Li, Y. Jiao, B. Barbiellini, A. Bansil, and H. Zhu, Condensed Matter **4**, 53 (2019).
- [9] J. T. Ye, Y. J. Zhang, R. Akashi, M. S. Bahramy, R. Arita, and Y. Iwasa, Science **338**, 1193 (2012).
- [10] W. Zhou, X. Zou, S. Najmaei, Z. Liu, Y. Shi, J. Kong, J. Lou, P. M. Ajayan, B. I. Yakobson, and J.-C. Idrobo, Nano letters **13**, 2615 (2013).
- [11] J. Jiang, T. Xu, J. Lu, L. Sun, and Z. Ni, Research (2019).
- [12] N. Mounet, M. Gibertini, P. Schwaller, D. Campi, A. Merkys, A. Marrazzo, T. Sohier, I. E. Castelli, A. Cepellotti, G. Pizzi, *et al.*, Nature nanotechnology **13**, 246 (2018).
- [13] G. Cheon, K.-A. N. Duerloo, A. D. Sendek, C. Porter, Y. Chen, and E. J. Reed, Nano letters **17**, 1915 (2017).
- [14] S. Haastrup, M. Strange, M. Pandey, T. Deilmann, P. S. Schmidt, N. F. Hinsche, M. N. Gjerding, D. Torelli, P. M. Larsen, A. C. Riis-Jensen, *et al.*, 2D Materials **5**, 042002 (2018).
- [15] F. A. Rasmussen and K. S. Thygesen, The Journal of Physical Chemistry C **119**, 13169 (2015).

[16] J. Zhou, L. Shen, M. D. Costa, K. A. Persson, S. P. Ong, P. Huck, Y. Lu, X. Ma, Y. Chen, H. Tang, *et al.*, *Scientific data* **6**, 86 (2019).

[17] A. C. Ferrari, F. Bonaccorso, V. Fal'Ko, K. S. Novoselov, S. Roche, P. Bøggild, S. Borini, F. H. Koppens, V. Palermo, N. Pugno, *et al.*, *Nanoscale* **7**, 4598 (2015).

[18] W. Witczak-Krempa, G. Chen, Y. B. Kim, and L. Balents, *Annu. Rev. Condens. Matter Phys.* **5**, 57 (2014).

[19] A. C. Hewson, *The Kondo problem to heavy fermions*, 2 (Cambridge university press, 1997).

[20] I. S. Sokolov, D. V. Averyanov, O. E. Parfenov, I. A. Karateev, A. N. Taldenkov, A. M. Tokmachev, and V. G. Storchak, *Materials Horizons* **7**, 1372 (2020).

[21] Z. Du, S. Yang, S. Li, J. Lou, S. Zhang, S. Wang, B. Li, Y. Gong, L. Song, X. Zou, *et al.*, *Nature* **577**, 492 (2020).

[22] K. Krämer, H. Güdel, P. Fischer, and L. Keller, *Applied Physics A* **74**, s595 (2002).

[23] D. Chen, S. Zhang, H. Yang, J. Li, and G. Chen, *Journal of Physics: Condensed Matter* **29**, 265803 (2017).

[24] R. Okuma, C. Ritter, G. J. Nilsen, and Y. Okada, *Physical Review Materials* **5**, L121401 (2021).

[25] B. G. Jang, C. Lee, J.-X. Zhu, and J. H. Shim, *npj 2D Materials and Applications* **6**, 80 (2022).

[26] V. A. Posey, S. Turkel, M. Rezaee, A. Devarakonda, A. K. Kundu, C. S. Ong, M. Thinel, D. G. Chica, R. A. Vitalone, R. Jing, *et al.*, *Nature* **625**, 483 (2024).

[27] N. Ru and I. Fisher, *Physical Review B—Condensed Matter and Materials Physics* **73**, 033101 (2006).

[28] H. You, N. Ding, J. Chen, X. Yao, and S. Dong, *ACS Applied Electronic Materials* **4**, 3168 (2022).

[29] Y. Yao, Y. Zhang, W. Xiong, Z. Wang, M. G. Sendeku, N. Li, J. Wang, W. Huang, F. Wang, X. Zhan, *et al.*, *Advanced Functional Materials* **29**, 1903017 (2019).

[30] P. Chen, W. Han, M. Zhao, J. Su, Z. Li, D. Li, L. Pi, X. Zhou, and T. Zhai, *Advanced Functional Materials* **31**, 2008790 (2021).

[31] J. You, Y. Luo, J. Yang, J. Zhang, K. Yin, K. Wei, X. Zheng, and T. Jiang, *Laser & Photonics Reviews* **14**, 2000239 (2020).

[32] C. Liu, J. Guo, L. Yu, J. Li, M. Zhang, H. Li, Y. Shi, and D. Dai, *Light: Science & Applications* **10**, 123 (2021).

[33] Z. Cheng, R. Cao, K. Wei, Y. Yao, X. Liu, J. Kang, J. Dong, Z. Shi, H. Zhang, and X. Zhang, *Advanced Science* **8**, 2003834 (2021).

[34] P. Blaha, K. Schwarz, P. Sorantin, and S. Trickey, *Computer physics communications* **59**, 399 (1990).

[35] P. Blaha, K. Schwarz, G. K. Madsen, D. Kvasnicka, J. Luitz, *et al.*, *An augmented plane wave+ local orbitals program for calculating crystal properties* **60** (2001).

[36] P. Blaha, K. Schwarz, F. Tran, R. Laskowski, G. K. Madsen, and L. D. Marks, *The Journal of chemical physics* **152** (2020).

[37] J. P. Perdew, K. Burke, and M. Ernzerhof, *Physical review letters* **77**, 3865 (1996).

[38] S. Alvarez, *Dalton Transactions* **42**, 8617 (2013).

[39] H. Hafiz, A. I. Khair, H. Choi, A. Mueen, A. Bansil, S. Eidenbenz, J. Wills, J.-X. Zhu, A. V. Balatsky, and T. Ahmed, *npj Computational Materials* **4**, 63 (2018).

ACKNOWLEDGEMENTS

This work was carried out under the auspices of the U.S. Department of Energy (DOE) National Nuclear Security Administration under Contract No. 89233218CNA000001. It was supported by the LANL LDRD Program, and in part by the Center for Integrated Nanotechnologies, a DOE BES user facility, in partnership with the LANL Institutional Computing Program for computational resources. Additional computations were performed at the National Energy Research Scientific Computing Center (NERSC), a U.S. Department of Energy Office of Science User Facility located at Lawrence Berkeley National Laboratory, operated under Contract No. DE-AC02-05CH11231 using NERSC award ERCAP0028014.

AUTHOR CONTRIBUTIONS

C.L. conceived and designed the study. C.L and L.H. proposed the computational framework and workflow. L.H. performed the first principles calculations. C.L., L.H. and Y.W.L. analysis the data and wrote the manuscript.

COMPETING INTERESTS

The authors declare no competing interests.

ADDITIONAL INFORMATION

Supplementary material in SM.pdf

Supplementary Material: High-Throughput Search and Prediction of Layered 4f-Materials

Lin Hou,¹ Ying Wai Li,² and Christopher Lane^{1,*}

¹*Theoretical Division, Los Alamos National Laboratory, Los Alamos, New Mexico 87545, USA*

²*Computer, Computational, and Statistical Sciences Division,
Los Alamos National Laboratory, Los Alamos, New Mexico 87545, USA*

(Dated: September 10, 2024)

I. COMPUTATION DETAILS

The $R_{mt}K_{max}$ used in the self-consistent density functional theory calculations follows the ‘rule of thumb’ given in Table. I

$R_{mt}K_{max}$	Smallest Atom In Unit Cell
3.0	H
4.5	Li
5.0	Be, B, Si
5.5	C, P
6.0	N, S
6.5	O, Cl, Na, K, Rb, Cs, Mg, Ca, Sr, Ba, Al
7.0	F
7.5	Sc-Cr, Ga-Br, Y-Mo
8.0	Mn-Zn, Ru-Cd, In-I, La, Ce, Hf-Re
8.5	Os-At, Pr-Lu, Ac-Lr

II. DATA TABLE

Table I presents the chemical, structural, and electronic information for the various layered 4f-materials, along with their database collection IDs. The band gap is given by value and type, i.e. indirect or direct, or if zero is indicated as a metal. If a specific calculation scenario would not converge a dash ‘-’ is used.

TABLE I: Data Table for all 295 Layered 4f Materials

ID	Chemical Formula	Database ID	Database ID	SG No.	SG Name	Non-SOC f in valence	SOC f in valence	Non-SOC f in Core	SOC f in Core
						Gap (Type)	Gap (Type)	Gap (Type)	Gap (Type)
1	ClH_2O_2Tb	COD	4315693	11	$P2_1/m$	–	–	–	–
2	$ClDyH_2O_2$	COD	4315694	11	$P2_1/m$	–	–	–	–
3	$PrTe_3$	COD	4124102	40	$Ama2$	0.0	0.0	0.0	0.0
4	I_5La_2	COD	8100408	11	$P2_1/m$	0.0	0.0	0.0	0.0
5	$ILuO$	COD	2216822	129	$P4/nmm$	3.268 (I)	3.047 (I)	3.277 (I)	3.033 (I)
6	$BrOPr$	COD	2232654	129	$P4/nmm$	0.0	0.0	4.337 (D)	4.174 (D)
7	$NdTe_3$	COD	4110942	63	$Cmcm$	0.0	0.0	0.0	0.0
8	Er_4I_5	COD	1529631	12	$C2/m$	0.0	0.0	0.0	0.0
9	Cl_3Er	COD	6000034	12	$C2/m$	0.0	0.0	4.749 (I)	4.717 (I)
10	AlF_6LiYb	COD	1519034	164	$P\bar{3}m1$	0.0	0.0	0.0	0.0
11	ClH_2LuO_2	COD	4315702	62	$Pnma$	4.880 (D)	4.838 (D)	4.871 (D)	4.833 (D)
12	$ILaO$	COD	9009171	129	$P4/nmm$	3.373 (D)	2.848 (D)	3.373 (D)	2.848 (D)
13	Cl_6HoNa_3	COD	8100894	14	$P2_1/c$	0.0	0.0	5.339 (D)	5.319 (D)
14	$H_6O_6P_3Yb$	COD	4322543	12	$C2/m$	–	–	–	–
15	$EuKPS_4$	COD	4319727	62	$Pnma$	0.0	0.0	0.0	0.0
16	ClH_2O_2Yb	COD	4315698	11	$P2_1/m$	0.0	0.0	4.788 (D)	4.750 (D)
17	$BrNdO$	COD	9009172	129	$P4/nmm$	0.0	0.0	4.184 (D)	4.034 (D)
18	$HoTe_3$	COD	4110939	63	$Cmcm$	0.0	0.0	0.0	0.0

Continued on next page. , I=Indirect Band Gap, D=Direct Band Gap, ‘-’ = Not Converged

TABLE I MM continued from previous page

ID	Chemical Formula	Database	Database ID	SG No.	SG Name	NonMSOC	SOC	NonMSOC	SOC
						f in valence Gap (Type)	f in valence Gap (Type)	f in Core Gap (Type)	f in Core Gap (Type)
19	$C_8H_{12}F_2O_{12}Tb_2$	COD	4329682	12	$C2/m$	—	—	—	—
20	$BrLaO$	COD	1530049	129	$P4/nmm$	3.717 (D)	3.551 (D)	3.717 (D)	3.551 (D)
21	ClH_2HoO_2	COD	4315695	11	$P2_1/m$	—	—	—	—
22	$IOPr$	COD	1530611	129	$P4/nmm$	0.0	0.0	3.753 (D)	3.398 (I)
23	$IOTm$	COD	2310429	129	$P4/nmm$	0.0	0.0	3.553 (I)	3.256 (I)
24	Te_3Tm	COD	4110941	63	$Cmcm$	0.0	0.0	0.0	0.0
25	KSe_2Yb	COD	8100307	166	$R\bar{3}m$	0.0	0.0	2.008 (I)	1.838 (I)
26	$Ho_2O_{13}Te_5$	COD	1532259	2	$P\bar{1}$	0.0	0.0	3.173 (I)	3.135 (I)
27	$ClErH_2O_2$	COD	4315696	11	$P2_1/m$	0.0	0.0	4.721 (D)	4.687 (D)
28	ClH_2O_2Tm	COD	4315700	62	$Pnma$	0.0	0.0	4.826 (D)	4.790 (D)
29	$TbCl_3$	ICSD	63543	166	$R\bar{3}m$	0.0	0.0	4.311 (D)	4.287 (D)
30	Sm	COD	9010999	194	$P6_3/mmc$	0.0	0.0	0.0	0.0
31	$ClErH$	COD	1530725	166	$R\bar{3}m$	0.0	0.0	0.0	0.0
32	$BrOSm$	COD	1530050	129	$P4/nmm$	0.0	0.0	4.391 (D)	4.259 (D)
33	$ErTe_3$	COD	4110940	63	$Cmcm$	0.0	0.0	0.0	0.0
34	$BrLuO$	COD	2214421	129	$P4/nmm$	4.171 (I)	4.048 (I)	4.223 (I)	4.093 (I)
35	I_2La	COD	1529708	139	$I4/mmm$	0.0	0.0	0.0	0.0
36	$SmTe_3$	COD	4110943	63	$Cmcm$	0.0	0.0	0.0	0.0
37	$EuK_4P_2S_8$	COD	4319726	72	$Ibam$	0.0	0.0	0.0	0.0
38	ClH_2O_2Sm	COD	2012446	62	$Pnma$	0.0	0.0	4.787 (D)	4.757 (D)
39	$CeH_2O_6P_2$	COD	2242273	164	$P\bar{3}m1$	—	—	—	—
40	ClH_2O_2Yb	COD	4315701	62	$Pnma$	0.0	0.0	4.575 (D)	4.543 (D)
41	Gd	COD	1526591	47	$Pmmm$	—	—	—	—
42	$ISSm$	COD	1008317	166	$R\bar{3}m$	0.0	0.0	1.693 (I)	1.502 (I)
43	ClH_2LuO_2	COD	4315699	11	$P2_1/m$	4.802 (D)	4.759 (D)	4.799 (D)	4.760 (D)
44	ClH_2O_2Tm	COD	4315697	11	$P2_1/m$	—	—	—	—
45	$CeTe_3$	COD	4124101	40	$Ama2$	0.0	0.0	0.0	0.0
46	$EuKPSe_4$	COD	4319720	62	$Pnma$	—	—	—	—
47	CCl_2Lu_2	ICSD	62227	166	$R\bar{3}m$	0.930 (I)	0.910 (I)	1.099 (I)	1.087 (I)
48	$ClLa$	ICSD	24410	166	$R\bar{3}m$	0.0	0.0	0.0	0.0
49	CBr_2Gd_2	ICSD	47226	164	$P\bar{3}m1$	0.0	0.0	0.0	0.0
50	LaS	ICSD	77831	64	$Cmce$	0.0	0.0	0.0	0.0
51	Ce_2Te_5	ICSD	622257	63	$Cmcm$	0.0	0.0	0.0	0.0
52	EuI_4La	ICSD	413999	15	$C2/c$	0.0	0.0	0.0	0.0
53	$CaInSe_4Yb$	ICSD	67654	62	$Pnma$	0.0	0.0	1.784 (I)	1.641 (I)
54	Ho_2Te_5	ICSD	639768	63	$Cmcm$	0.0	0.0	0.0	0.0
55	AgP_2Se_6Tm	ICSD	420304	163	$P\bar{3}1c$	0.0	0.0	1.672 (I)	1.654 (I)
56	$C_2Br_5La_4$	ICSD	418409	71	$Immm$	—	—	—	—
57	$H_8CeO_7P_3$	ICSD	88339	2	$P\bar{1}$	—	—	—	—
58	Ag_2Nd	ICSD	58339	191	$P6/mmm$	0.0	0.0	0.0	0.0
59	$Dy_2O_{13}Te_5$	ICSD	413664	2	$P\bar{1}$	—	—	—	—
60	$CaClCuO_3Sm$	ICSD	86428	129	$P4/nmm$	0.0	0.0	0.0	0.0
61	Cl_3Dy	ICSD	40064	63	$Cmcm$	0.0	0.0	3.620 (I)	3.590 (I)
62	I_4LaSm	ICSD	413996	15	$C2/c$	0.0	0.083 (I)	0.0	0.083 (I)
63	$KNdO_8S_2$	ICSD	65620	14	$P2_1/c$	—	—	—	—
64	$HClLu$	ICSD	62226	166	$R\bar{3}m$	0.0	0.0	0.0	0.0
65	$EuIO$	ICSD	27666	129	$P4/nmm$	0.0	0.299 (D)	3.518 (I)	3.166 (I)
66	Te_5Tm_2	ICSD	653111	63	$Cmcm$	0.0	0.0	0.0	0.0
67	$CuPbSe_3Tb$	ICSD	152516	62	$Pnma$	0.0	0.0	1.281 (I)	1.035 (I)
68	$BiLaOS_2$	ICSD	252466	129	$P4/nmm$	0.0	0.0	0.0	0.0
69	As_2CeLi_2	ICSD	32042	164	$P\bar{3}m1$	0.375 (I)	0.339 (I)	0.0	0.0
70	CeI_4Sr	ICSD	413997	15	$C2/c$	0.0	0.0	0.097 (I)	0.095 (I)
71	$AgErP_2Se_6$	ICSD	420303	163	$P\bar{3}1c$	0.0	0.0	1.662 (I)	1.644 (I)
72	$DyTe_3$	ICSD	630328	63	$Cmcm$	0.0	0.0	0.0	0.0
73	Br_5Pr_2	ICSD	72801	11	$P2_1/m$	0.0	0.0	0.0	0.0
74	$LaSeTe_2$	ICSD	413173	63	$Cmcm$	0.0	0.0	0.0	0.0

Continued on next page. , I=Indirect Band Gap, D=Direct Band Gap, '-' = Not Converged

TABLE I MM continued from previous page

ID	Chemical Formula	Database	Database ID	SG No.	SG Name	NonMSOC	SOC	NonMSOC	SOC
						f in valence Gap (Type)	f in valence Gap (Type)	f in Core Gap (Type)	f in Core Gap (Type)
75	I_3Km	ICSD	72343	63	$Cmcm$	0.0	0.0	0.0	0.0
76	$CITb$	ICSD	23351	166	$R\bar{3}m$	0.0	0.0	0.0	0.0
77	La_2Te_5	ICSD	642015	63	$Cmcm$	0.0	0.0	0.0	0.0
78	$C_2Br_5Ce_4$	ICSD	418408	71	$Immm$	0.0	0.0	0.0	0.0
79	$CuDyPbSe_3$	ICSD	152517	62	$Pnma$	0.0	0.0	1.238 (I)	0.967 (I)
80	$CuPbSe_3Yb$	ICSD	152521	62	$Pnma$	0.0	0.0	1.210 (I)	0.966 (I)
81	I_2Tm	ICSD	43731	164	$P\bar{3}m1$	0.0	0.0	0.0	0.0
82	Al_2Cl_8Sm	ICSD	56731	13	$P12/a1$	0.190 (D)	0.334 (D)	0.0	0.0
83	$BiCeOS_2$	ICSD	80	129	$P4/nmm$	0.0	0.0	0.562 (I)	0.299 (I)
84	$ClErS$	ICSD	21009	59	$Pmmn$	—	—	—	—
85	$CeLi_2P_2$	ICSD	42016	164	$P\bar{3}m1$	0.327 (I)	0.265 (I)	0.0	0.0
86	Li_2P_2Pr	ICSD	23259	164	$P\bar{3}m1$	0.0	0.0	0.0	0.509 (I)
87	GeI_2La_2	ICSD	414171	166	$R\bar{3}m$	—	—	—	—
88	$H_{0.8}GdI$	ICSD	61035	166	$R\bar{3}m$	0.0	0.0	0.0	0.0
89	$CuLuPbSe_3$	ICSD	152522	62	$Pnma$	1.119 (I)	0.882 (I)	1.156 (I)	0.924 (I)
90	$BrOYb$	ICSD	28532	129	$P4/nmm$	0.0	0.0	4.237 (I)	4.109 (I)
91	H_2ClLaO_2	ICSD	6280	10	$P2/m$	0.148 (I)	0.147 (I)	0.148 (I)	0.147 (I)
92	$LuTe_3$	ICSD	642621	63	$Cmcm$	0.0	0.0	0.0	0.0
93	$CuErPbSe_3$	ICSD	152519	62	$Pnma$	0.0	0.0	1.200 (I)	0.975 (I)
94	$HLaNb_2O_7$	ICSD	72567	123	$P4/mmm$	0.0	0.0	0.0	0.0
95	Sm_2Te_5	ICSD	652655	63	$Cmcm$	0.0	0.0	0.0	0.0
96	I_2Nd	ICSD	72190	139	$I4/mmm$	0.0	0.0	0.0	0.0
97	$BrEuO$	ICSD	28531	129	$P4/nmm$	0.0	0.318 (I)	4.338 (D)	4.219 (D)
98	$K_4P_4S_{14}Sm_2$	ICSD	161010	5	$C2$	0.0	0.0	0.0	0.0
99	$H_5NdO_8Se_2$	ICSD	78051	19	$P2_{1}2_{1}2_{1}$	—	—	—	—
100	$CuPbSe_3Yb$	ICSD	154613	62	$Pnma$	0.0	0.0	1.186 (I)	0.937 (I)
101	$CeCuKT_4$	ICSD	86654	59	$Pmmn$	0.0	0.0	0.0	0.0
102	$GdIS$	ICSD	416462	59	$Pmmn$	—	—	—	—
103	$ErIS$	ICSD	50194	59	$Pmmn$	—	—	—	—
104	$C_2H_7GdO_8S$	ICSD	163610	2	$P\bar{1}$	—	—	—	—
105	Dy_2Te_5	ICSD	630329	63	$Cmcm$	0.0	0.0	0.0	0.0
106	$BrLa$	ICSD	23354	166	$R\bar{3}m$	0.0	0.0	0.0	0.0
107	$BrTb$	ICSD	23353	166	$R\bar{3}m$	0.0	0.0	0.0	0.0
108	I_2La_2Te	ICSD	240698	166	$R\bar{3}m$	0.0	0.0	0.0	0.0
109	$Ge_2I_2La_2$	ICSD	59801	164	$P\bar{3}m1$	0.0	0.0	0.0	0.0
110	$NdSeTe_2$	ICSD	391289	63	$Cmcm$	0.0	0.0	0.0	0.0
111	I_3La	ICSD	31596	63	$Cmcm$	1.523 (I)	1.264 (I)	1.523 (I)	1.264 (I)
112	Br_2La	ICSD	65481	194	$P6_3/mmc$	0.0	0.0	0.0	0.0
113	$PrSeTe_2$	ICSD	412465	63	$Cmcm$	0.0	0.0	0.0	0.0
114	As_2Li_2Nd	ICSD	23261	164	$P\bar{3}m1$	0.0	0.0	0.0	0.0
115	Al_2Cl_8Eu	ICSD	56734	13	$P12/a1$	0.0	0.0	0.0	0.0
116	$O_{13}Te_5Yb_2$	ICSD	413668	2	$P\bar{1}$	—	—	—	—
117	LaS	ICSD	69581	39	$Abm2$	0.0	0.0	0.0	0.0
118	$I_2La_2O_4Si$	ICSD	72654	14	$P2_{1}/c$	—	—	—	—
119	$CuPbSe_3Tm$	ICSD	152520	62	$Pnma$	—	—	—	—
120	Cu_2EuKT_4	ICSD	280193	99	$P4/mm$	—	—	—	—
121	Br_2La_2P	ICSD	418009	164	$P\bar{3}m1$	0.0	0.0	0.0	0.0
122	$LaTe_3$	ICSD	642056	63	$Cmcm$	0.0	0.0	0.0	0.0
123	$Ce_2I_2Si_2$	ICSD	407246	164	$P\bar{3}m1$	0.0	0.0	0.0	0.0
124	As_2Li_2Pr	ICSD	23260	164	$P\bar{3}m1$	0.0	0.0	0.0	0.0
125	Nd_2Te_5	ICSD	24181	63	$Cmcm$	0.0	0.0	0.0	0.0
126	$DyIS$	ICSD	79107	59	$Pmmn$	—	—	—	—
127	$O_{13}Te_5Tm_2$	ICSD	413667	2	$P\bar{1}$	—	—	—	—
128	$Er_2O_{13}Te_5$	ICSD	413666	2	$P\bar{1}$	—	—	—	—
129	$H_4I_3O_{11}Sm$	ICSD	250551	2	$P\bar{1}$	—	—	—	—
130	I_2Yb	ICSD	77907	164	$P\bar{3}m1$	0.724 (I)	0.303 (I)	0.0	0.0

Continued on next page. , I=Indirect Band Gap, D=Direct Band Gap, '—' = Not Converged

TABLE I MM continued from previous page

ID	Chemical Formula	Database	Database ID	SG No.	SG Name	NonMSOC	SOC	NonMSOC	SOC
						f in valence Gap (Type)	f in valence Gap (Type)	f in Core Gap (Type)	f in Core Gap (Type)
131	<i>KLaP₂Se₆</i>	ICSD	81300	14	<i>P2₁/c</i>	2.062 (I)	2.039 (I)	2.062 (I)	2.039 (I)
132	<i>CuHoPbSe₃</i>	ICSD	154669	62	<i>Pnma</i>	0.0	0.0	1.251 (I)	0.998 (I)
133	<i>La₂P₄S₁₄Tl₄</i>	ICSD	195314	12	<i>C2/m</i>	2.060 (I)	2.021 (I)	2.060 (I)	2.021 (I)
134	<i>ClTb</i>	ICSD	23352	166	<i>R₃m</i>	0.0	0.0	0.0	0.0
135	<i>I₂La₂P</i>	ICSD	418010	164	<i>P₃m1</i>	0.0	0.0	0.0	0.0
136	<i>Pr₂Te₅</i>	ICSD	649404	63	<i>Cmcm</i>	0.0	0.0	0.0	0.0
137	<i>TbTe₃</i>	ICSD	652952	63	<i>Cmcm</i>	0.0	0.0	0.0	0.0
138	<i>GeI₂La₂</i>	ICSD	414170	164	<i>P₃m1</i>	0.311 (I)	0.234 (I)	0.311 (I)	0.234 (I)
139	<i>BrDyS</i>	ICSD	79106	59	<i>Pmmn</i>	—	—	—	—
140	<i>Br₅Ce₂</i>	ICSD	167088	11	<i>P2₁/m</i>	0.0	0.0	0.0	0.0
141	<i>HoIS</i>	ICSD	425285	59	<i>Pmmn</i>	—	—	—	—
142	<i>ClOYb</i>	ICSD	6077	166	<i>R₃m</i>	0.0	0.0	4.485 (I)	4.458 (I)
143	<i>Cl₄Cu₃O₁₂Te₄Yb₂</i>	ICSD	419113	2	<i>P₁</i>	—	—	—	—
144	<i>KPrSe₄Si</i>	ICSD	416622	4	<i>P2₁(No.4)</i>	0.0	0.0	0.0	0.0
145	<i>LuPS₄</i>	ICSD	412857	14	<i>P2₁/c</i>	2.091 (D)	2.084 (D)	2.107 (D)	2.100 (D)
146	<i>Br₃Nd</i>	ICSD	31590	63	<i>Cmcm</i>	0.0	0.0	2.241 (I)	2.128 (I)
147	<i>Lu₂O₁₃Te₅</i>	ICSD	413669	2	<i>P₁</i>	3.098 (I)	3.061 (I)	3.144 (I)	3.110 (I)
148	<i>La₂SiO₄I₂</i>	MPDS	s1502676	2	<i>P₁</i>	—	—	—	—
149	<i>TbSeI</i>	MPDS	s376106	59	<i>Pmmn</i>	—	—	—	—
150	<i>ErClO</i>	MPDS	s1936405	166	<i>R₃m</i>	0.0	0.0	4.360 (I)	4.349 (I)
151	<i>YbSeI</i>	MPDS	s376101	59	<i>Pmmn</i>	—	—	—	—
152	<i>SmI₃</i>	MPDS	s1300329	63	<i>Cmcm</i>	0.0	0.0	1.430 (I)	1.154 (I)
153	<i>ErSbS₂O</i>	MPDS	s1237956	129	<i>P4/nmm</i>	0.0	0.0	0.308 (I)	0.158 (I)
154	<i>LaSiI</i>	MPDS	s1902101	164	<i>P₃m1</i>	0.0	0.0	0.0	0.0
155	<i>NaHoCl₄</i>	MPDS	s1707979	2	<i>P₁</i>	0.0	0.0	4.670 (I)	4.638 (I)
156	<i>SrTbF₆</i>	MPDS	s1827765	67	<i>Cmme</i>	0.0	0.0	0.0	0.0
157	<i>LuSI</i>	MPDS	s1937399	59	<i>Pmmn</i>	—	—	—	—
158	<i>LaCBr</i>	MPDS	s1227665	12	<i>C2/m</i>	—	—	—	—
159	<i>PrSI</i>	MPDS	s1703862	166	<i>R₃m</i>	0.0	0.0	1.706 (I)	1.521 (I)
160	<i>TmCl₃</i>	MPDS	s1300748	12	<i>C2/m</i>	0.0	0.0	5.118 (I)	5.087 (I)
161	<i>LuCl₃</i>	MPDS	s542066	167	<i>R₃2/c</i>	4.513 (I)	4.391 (D)	4.626 (I)	4.537 (D)
162	<i>EuIH</i>	MPDS	s1937757	129	<i>P4/nmm</i>	0.0	0.0	0.0	0.0
163	<i>GdB₂S₂O</i>	MPDS	s309739	129	<i>P4/nmm</i>	0.0	0.0	0.580 (I)	0.278 (I)
164	<i>HoBr</i>	MPDS	s542057	166	<i>R₃m</i>	0.0	0.0	0.0	0.0
165	<i>CaCuEuClO₃</i>	MPDS	s1900579	129	<i>P4/nmm</i>	0.0	0.0	0.0	0.0
166	<i>DyBrO</i>	MPDS	s1903365	129	<i>P4/nmm</i>	0.0	0.0	0.0	0.0
167	<i>PrBiS₂O</i>	MPDS	s307830	129	<i>P4/nmm</i>	0.0	0.0	0.415 (I)	0.105 (I)
168	<i>DySbS₂O</i>	MPDS	s1237954	129	<i>P4/nmm</i>	0.0	0.0	0.309 (D)	0.180 (I)
169	<i>HoCl₃</i>	MPDS	s1300746	12	<i>C2/m</i>	0.0	0.0	5.053 (I)	5.024 (I)
170	<i>GdSI</i>	MPDS	s1703873	166	<i>R₃m</i>	0.0	0.0	1.727 (I)	1.529 (I)
171	<i>ErBr</i>	MPDS	s542062	166	<i>R₃m</i>	0.0	0.0	0.0	0.0
172	<i>DySI</i>	MPDS	s1703875	166	<i>R₃m</i>	0.0	0.0	1.738 (I)	1.533 (I)
173	<i>CeBrO</i>	MPDS	s1903359	129	<i>P4/nmm</i>	—	—	—	—
174	<i>NdB₂S₂O</i>	MPDS	s309736	129	<i>P4/nmm</i>	0.0	0.0	0.557 (I)	0.248 (I)
175	<i>DyBiS₂O</i>	MPDS	s309735	129	<i>P4/nmm</i>	0.0	0.0	0.541 (I)	0.215 (I)
176	<i>HoClO</i>	MPDS	s1936402	166	<i>R₃m</i>	0.0	0.0	3.395 (I)	3.323 (I)
177	<i>YbI₃</i>	MPDS	s1300578	148	<i>R₃</i>	0.0	0.0	2.719 (I)	2.379 (I)
178	<i>GdSeI</i>	MPDS	s376100	59	<i>Pmmn</i>	—	—	—	—
179	<i>GdSbS₂O</i>	MPDS	s1237952	129	<i>P4/nmm</i>	0.0	0.0	0.285 (D)	0.190 (D)
180	<i>LuI₃</i>	MPDS	s1300579	148	<i>R₃</i>	2.713 (I)	2.362 (I)	2.753 (I)	2.404 (I)
181	<i>GdCl₃</i>	MPDS	s1301084	63	<i>Cmcm</i>	0.0	0.0	2.928 (I)	2.902 (I)
182	<i>ErSBr</i>	MPDS	s307276	59	<i>Pmmn</i>	—	—	—	—
183	<i>NaDyCl₄</i>	MPDS	s1707978	2	<i>P₁</i>	0.0	0.0	4.650 (I)	4.618 (I)
184	<i>LuSeI</i>	MPDS	s376107	59	<i>Pmmn</i>	—	—	—	—
185	<i>NdSbS₂O</i>	MPDS	s307831	129	<i>P4/nmm</i>	0.0	0.0	0.330 (D)	0.243 (D)
186	<i>HoBr₃</i>	MPDS	s1300321	63	<i>Cmcm</i>	0.0	0.0	2.220 (I)	2.097 (I)

Continued on next page. , I=Indirect Band Gap, D=Direct Band Gap, '-' = Not Converged

TABLE I MM continued from previous page

ID	Chemical Formula	Database	Database ID	SG No.	SG Name	NonMSOC	SOC	NonMSOC	SOC
						f in valence Gap (Type)	f in valence Gap (Type)	f in Core Gap (Type)	f in Core Gap (Type)
187	<i>YbSI</i>	MPDS	s1937398	59	<i>Pmmn</i>	—	—	—	—
188	<i>Gd₂GeBr₂</i>	MPDS	s1923103	164	<i>P$\bar{3}m1$</i>	0.0	0.0	0.050 (I)	0.0
189	<i>GdI₂</i>	MPDS	s1300639	194	<i>P6₃/mmc</i>	0.0	0.0	0.0	0.0
190	<i>EuIF</i>	MPDS	s1800106	129	<i>P4/nmm</i>	0.0	0.0	0.0	0.0
191	<i>DyAsO₄</i>	MPDS	s1925690	74	<i>Imma</i>	0.0	0.0	2.933 (I)	2.932 (I)
192	<i>TmSeF</i>	MPDS	s307728	166	<i>R$\bar{3}m$</i>	0.0	0.0	3.004 (I)	2.949 (I)
193	<i>ErClO</i>	MPDS	s1936404	166	<i>R$\bar{3}m$</i>	0.0	0.0	3.447 (I)	3.374 (I)
194	<i>PrI₃</i>	MPDS	s1300568	63	<i>Cmcm</i>	—	—	—	—
195	<i>LaI</i>	MPDS	s1301547	166	<i>R$\bar{3}m$</i>	0.0	0.0	0.0	0.0
196	<i>ErBrO</i>	MPDS	s1903357	129	<i>P4/nmm</i>	0.0	0.0	3.575 (I)	3.554 (I)
197	<i>TbVO₄</i>	MPDS	s1925692	15	<i>C2/c</i>	0.0	0.0	0.0	0.0
198	<i>LaCl</i>	MPDS	s1936154	12	<i>C2/m</i>	—	—	—	—
199	<i>GdI₃</i>	MPDS	s1300318	63	<i>Cmcm</i>	0.0	0.0	1.464 (I)	1.181 (I)
200	<i>YbCl₃</i>	MPDS	s1301310	63	<i>Cmcm</i>	0.0	0.0	2.924 (I)	2.892 (I)
201	<i>YbIF</i>	MPDS	s1800112	129	<i>P4/nmm</i>	0.405 (I)	0.138 (I)	0.0	0.0
202	<i>DyVO₄</i>	MPDS	s1925691	74	<i>Imma</i>	0.0	0.0	2.502 (I)	2.501 (I)
203	<i>LuSBr</i>	MPDS	s307274	59	<i>Pmmn</i>	—	—	—	—
204	<i>TmSeI</i>	MPDS	s376102	59	<i>Pmmn</i>	—	—	—	—
205	<i>TbBr₃</i>	MPDS	s1800615	12	<i>C2/m</i>	0.0	0.0	4.175 (I)	4.070 (I)
206	<i>DyBr₃</i>	MPDS	s1300320	63	<i>Cmcm</i>	0.0	0.0	2.208 (I)	2.087 (I)
207	<i>YbI₃O₉H₄O₂</i>	MPDS	s1711735	2	<i>P$\bar{1}$</i>	—	—	—	—
208	<i>ErIO</i>	MPDS	s383717	129	<i>P4/nmm</i>	0.0	0.0	0.0	0.0
209	<i>La₂SbI₂</i>	MPDS	s1713664	164	<i>P$\bar{3}m1$</i>	0.0	0.0	0.0	0.0
210	<i>TbI₃</i>	MPDS	s1300319	63	<i>Cmcm</i>	0.0	0.0	1.459 (I)	1.168 (I)
211	<i>YbSBr</i>	MPDS	s307275	59	<i>Pmmn</i>	—	—	—	—
212	<i>TmBrF</i>	MPDS	s1800108	129	<i>P4/nmm</i>	0.0	0.0	0.0	0.0
213	<i>PrBr₃</i>	MPDS	s1300387	63	<i>Cmcm</i>	0.0	0.0	2.159 (I)	2.030 (I)
214	<i>HoSbS₂O</i>	MPDS	s1237955	129	<i>P4/nmm</i>	0.0	0.0	0.307 (D)	0.179 (I)
215	<i>GdBrO</i>	MPDS	s1903363	129	<i>P4/nmm</i>	0.0	0.0	0.0	0.0
216	<i>GdCBr</i>	MPDS	s1703258	12	<i>C2/m</i>	—	—	—	—
217	<i>LaBiSe₂O</i>	MPDS	s1833135	129	<i>P4/nmm</i>	0.107 (I)	0.0	0.107 (I)	0.0
218	<i>ErI₃</i>	MPDS	s1300576	148	<i>R$\bar{3}$</i>	0.0	0.0	2.658 (I)	2.320 (I)
219	<i>LuSbS₂O</i>	MPDS	s1237959	129	<i>P4/nmm</i>	0.132 (I)	0.0	0.332 (I)	0.171 (I)
220	<i>ErSeBr</i>	MPDS	s1701716	59	<i>Pmmn</i>	—	—	—	—
221	<i>TbCBr</i>	MPDS	s1702973	12	<i>C2/m</i>	—	—	—	—
222	<i>PrI₂</i>	MPDS	s1300557	139	<i>I4/mmm</i>	0.0	0.0	0.0	0.0
223	<i>GdI₃</i>	MPDS	s1300572	148	<i>R$\bar{3}$</i>	0.0	0.0	2.560 (I)	2.240 (I)
224	<i>Lu₂CBr₂</i>	MPDS	s1708510	166	<i>R$\bar{3}m$</i>	0.712 (I)	0.672 (I)	0.839 (I)	0.796 (I)
225	<i>ErSeF</i>	MPDS	s307729	166	<i>R$\bar{3}m$</i>	0.0	0.0	2.969 (I)	2.917 (I)
226	<i>TmSI</i>	MPDS	s1937397	59	<i>Pmmn</i>	—	—	—	—
227	<i>YbBr₃</i>	MPDS	s1800621	148	<i>R$\bar{3}$</i>	0.0	0.0	3.629 (I)	3.471 (I)
228	<i>NaTbCl₄</i>	MPDS	s1707977	2	<i>P$\bar{1}$</i>	0.134 (I)	0.0	4.635 (I)	4.605 (I)
229	<i>TmBrO</i>	MPDS	s1903367	129	<i>P4/nmm</i>	0.0	0.0	0.0	0.0
230	<i>SmIF</i>	MPDS	s1800103	129	<i>P4/nmm</i>	0.0	0.042 (I)	0.0	0.0
231	<i>EuBr_{2.99}</i>	MPDS	s1500132	63	<i>Cmcm</i>	0.058 (D)	0.169 (I)	2.203 (I)	2.092 (I)
232	<i>HoSeI</i>	MPDS	s376104	59	<i>Pmmn</i>	—	—	—	—
233	<i>TmBr₃</i>	MPDS	s1300335	148	<i>R$\bar{3}$</i>	0.0	0.0	3.588 (I)	3.436 (I)
234	<i>DyI₃</i>	MPDS	s1300574	148	<i>R$\bar{3}$</i>	0.0	0.0	2.604 (I)	2.272 (I)
235	<i>DyCl₃</i>	MPDS	s541787	12	<i>C2/m</i>	0.0	0.0	5.013 (I)	4.986 (I)
236	<i>TbI₃</i>	MPDS	s1300573	148	<i>R$\bar{3}$</i>	0.0	0.0	2.582 (I)	2.258 (I)
237	<i>CaCuGdClO₃</i>	MPDS	s1900577	129	<i>P4/nmm</i>	0.0	0.0	0.0	0.0
238	<i>YbBiS₂O</i>	MPDS	s309734	129	<i>P4/nmm</i>	0.0	0.0	0.553 (I)	0.226 (I)
239	<i>HoSBr</i>	MPDS	s307277	59	<i>Pmmn</i>	—	—	—	—
240	<i>NdI₃</i>	MPDS	s1300569	63	<i>Cmcm</i>	0.0	0.0	1.420 (I)	1.151 (I)
241	<i>NaEuCl₄</i>	MPDS	s1707975	2	<i>P$\bar{1}$</i>	0.180 (I)	0.460 (D)	4.612 (I)	4.584 (I)
242	<i>TbBrO</i>	MPDS	s1903364	129	<i>P4/nmm</i>	0.0	0.0	0.0	0.0

Continued on next page. , I=Indirect Band Gap, D=Direct Band Gap, '-' = Not Converged

TABLE I MM continued from previous page

ID	Chemical Formula	Database	Database ID	SG No.	SG Name	NonMSOC	SOC	NonMSOC	SOC
						f in valence Gap (Type)	f in valence Gap (Type)	f in Core Gap (Type)	f in Core Gap (Type)
243	<i>PrSbS₂O</i>	MPDS	s1237948	129	<i>P4/nmm</i>	0.0	0.0	0.331 (D)	0.244 (D)
244	<i>EuSbS₂O</i>	MPDS	s1237951	129	<i>P4/nmm</i>	0.0	0.0	0.297 (D)	0.199 (D)
245	<i>CeI₂</i>	MPDS	s1721470	139	<i>I4/mmm</i>	0.0	0.0	0.0	0.0
246	<i>Gd₂CCl₂</i>	MPDS	s1400313	164	<i>P₃m1</i>	0.0	0.0	0.812 (I)	0.772 (I)
247	<i>TmI₃</i>	MPDS	s1300577	148	<i>R₃</i>	0.0	0.0	2.691 (I)	2.344 (I)
248	<i>ErCl₃</i>	MPDS	s1301309	63	<i>Cmcm</i>	0.0	0.0	2.893 (I)	2.864 (I)
249	<i>GdGaI</i>	MPDS	s1623208	164	<i>P₃m1</i>	0.0	0.0	0.0	0.0
250	<i>ErBr₃</i>	MPDS	s1300334	148	<i>R₃</i>	0.0	0.0	3.549 (I)	3.402 (I)
251	<i>TmClO</i>	MPDS	s1936406	166	<i>R₃m</i>	0.0	0.0	3.470 (I)	3.396 (I)
252	<i>TbSI</i>	MPDS	s1937394	59	<i>Pmmn</i>	—	—	—	—
253	<i>TmClO</i>	MPDS	s1936407	166	<i>R₃m</i>	0.0	0.0	4.365 (I)	4.353 (I)
254	<i>HoSeF</i>	MPDS	s307730	166	<i>R₃m</i>	0.0	0.0	2.939 (I)	2.890 (I)
255	<i>GdTe₃</i>	MPDS	s525784	63	<i>Cmcm</i>	0.0	0.0	0.0	0.0
256	<i>CeSI</i>	MPDS	s1252944	61	<i>Pbca</i>	0.0	0.0	2.067 (D)	1.815 (D)
257	<i>LuSeF</i>	MPDS	s307726	166	<i>R₃m</i>	3.027 (I)	2.961 (I)	3.077 (I)	3.017 (I)
258	<i>ErSI</i>	MPDS	s1937396	59	<i>Pmmn</i>	—	—	—	—
259	<i>YbBrH</i>	MPDS	s1937759	129	<i>P4/nmm</i>	0.311 (I)	0.062 (I)	0.0	0.0
260	<i>PrI₂</i>	MPDS	s1300558	194	<i>P₆3/mmc</i>	0.0	0.0	0.0	0.0
261	<i>GdCl</i>	MPDS	s542059	166	<i>R₃m</i>	0.0	0.0	0.0	0.0
262	<i>SmBiS₂O</i>	MPDS	s309738	129	<i>P4/nmm</i>	0.0	0.0	0.587 (I)	0.276 (I)
263	<i>KLaP₂S₆</i>	MPDS	s1811367	14	<i>P₂1/c</i>	2.779 (I)	2.753 (I)	2.779 (I)	2.753 (I)
264	<i>HoI₃</i>	MPDS	s1300575	148	<i>R₃</i>	0.0	0.0	2.630 (I)	2.296 (I)
265	<i>YbSeF</i>	MPDS	s307727	166	<i>R₃m</i>	0.0	0.0	3.037 (I)	2.979 (I)
266	<i>HoBrO</i>	MPDS	s1903366	129	<i>P4/nmm</i>	0.0	0.0	0.0	0.0
267	<i>La₂AsI₂</i>	MPDS	s1713663	164	<i>P₃m1</i>	0.0	0.0	0.0	0.0
268	<i>YbSbS₂O</i>	MPDS	s1237958	129	<i>P4/nmm</i>	0.0	0.0	0.310 (D)	0.175 (I)
269	<i>SrCuNdClO₃</i>	MPDS	s1900576	129	<i>P4/nmm</i>	0.0	0.0	0.0	0.0
270	<i>TbSbS₂O</i>	MPDS	s1237953	129	<i>P4/nmm</i>	0.0	0.0	0.310 (I)	0.175 (I)
271	<i>DyI₂</i>	MPDS	s1707656	166	<i>R₃m</i>	0.0	0.0	0.0	0.0
272	<i>YbBrF</i>	MPDS	s1800111	129	<i>P4/nmm</i>	0.464 (I)	0.047 (I)	0.0	0.0
273	<i>GdB₃</i>	MPDS	s1300330	148	<i>R₃</i>	0.0	0.0	3.419 (I)	3.292 (I)
274	<i>SmI₃</i>	MPDS	s1300571	148	<i>R₃</i>	0.0	0.0	2.518 (I)	2.191 (I)
275	<i>DyBr₃</i>	MPDS	s1300332	148	<i>R₃</i>	0.0	0.0	3.487 (I)	3.347 (I)
276	<i>SmSbS₂O</i>	MPDS	s304255	129	<i>P4/nmm</i>	0.0	0.0	0.304 (D)	0.205 (D)
277	<i>Na₃LuCl₆</i>	MPDS	s1706468	14	<i>P₂1/c</i>	4.786 (D)	4.713 (D)	5.096 (I)	5.084 (I)
278	<i>SmIO</i>	MPDS	s1401116	129	<i>P4/nmm</i>	0.0	0.0	0.0	0.0
279	<i>TbGaI</i>	MPDS	s1623209	164	<i>P₃m1</i>	0.0	0.0	0.0	0.0
280	<i>NdSI</i>	MPDS	s1703863	166	<i>R₃m</i>	0.0	0.0	1.695 (I)	1.508 (I)
281	<i>YbCl₃</i>	MPDS	s1300376	12	<i>C₂/m</i>	0.0	0.0	5.136 (I)	5.103 (I)
282	<i>LaBiS₂O</i>	MPDS	s1641780	11	<i>P₂1/m</i>	0.207 (I)	0.048 (I)	0.207 (I)	0.048 (I)
283	<i>Gd₂GeI₂</i>	MPDS	s1923102	166	<i>R₃m</i>	0.0	0.0	0.116 (I)	0.0
284	<i>KYbI₃</i>	MPDS	s1710745	63	<i>Cmcm</i>	0.867 (D)	0.405 (D)	0.0	0.0
285	<i>NaGdCl₄</i>	MPDS	s1707007	2	<i>P₁</i>	0.0	0.0	4.618 (I)	4.589 (I)
286	<i>PrBr</i>	MPDS	s542061	166	<i>R₃m</i>	0.0	0.0	0.0	0.0
287	<i>SmBi₂Se₄</i>	MPDS	s543829	62	<i>Pnma</i>	—	—	—	—
288	<i>PrSiI</i>	MPDS	s1902103	164	<i>P₃m1</i>	0.0	0.0	0.0	0.0
289	<i>NdIO</i>	MPDS	s1140364	129	<i>P4/nmm</i>	0.0	0.0	0.0	0.0
290	<i>KLaSiSe₄</i>	MPDS	s537612	4	<i>P₂1</i> (No.4)	2.127 (I)	2.072 (I)	2.127 (I)	2.072 (I)
291	<i>TmSbS₂O</i>	MPDS	s1237957	129	<i>P4/nmm</i>	0.0	0.0	0.318 (D)	0.166 (I)
292	<i>LuBr₃</i>	MPDS	s1300337	148	<i>R₃</i>	3.605 (I)	3.443 (I)	3.669 (I)	3.507 (I)
293	<i>KDyI₃</i>	MPDS	s1711765	63	<i>Cmcm</i>	0.0	0.0	0.0	0.0
294	<i>HoBr₃</i>	MPDS	s1300333	148	<i>R₃</i>	0.0	0.0	3.517 (I)	3.517 (I)
295	<i>LaSbSe₂O</i>	MPDS	s1502067	129	<i>P4/nmm</i>	0.097 (I)	0.0	0.097 (I)	0.0

Continued on next page. , I=Indirect Band Gap, D=Direct Band Gap, '-' = Not Converged

TABLE I MM continued from previous page

ID	Chemical Formula	Database ID	Database ID	SG No.	SG Name	NonMSOC	SOC	NonMSOC	SOC
						f in valence	f in valence	f in Core	f in Core
						Gap (Type)	Gap (Type)	Gap (Type)	Gap (Type)

* laneca@lanl.gov